Supporting Information

Twin PdPtIr Porous Nanotubes as Dual-Functional Catalyst for Oxygen Reduction and Evolution Reactions

Dan Yu[1], Qian Liu[1], Bing Chen[1], Yisong Zhao[1], Peng Jia[1], Keju Sun[1,] *, Faming Gao[1,2,] *

[1]Hebei Key Laboratory of Applied Chemistry, Yanshan University, Qinhuangdao 066004, China

[2]Tianjin Key Laboratory of Brine Chemical Engineering and Resource Ecological Utilization, Tianjin University of Science & Technology, Tianjin 300222, P.R.China

Corresponding Author

*E-mail: gfm0827@sina.com (Faming Gao); sunkj@ysu.edu.cn (Keju Sun)

This PDF file includes:

1. Materials and reagents

Palladium chloride 59-60%, Iridium chloride 99.8%, ascorbic acid 99.99%, sodium iodide 99.99%, ethylene glycol (EG) 99.5% were purchased from Aladdin. Platinum (IV) chloride 99.99%, Nifion (5 wt%), perchloric acid (70%) 99.999% were purchased from Sigma-Aldrich. ethanol 99.9%, isopropyl alcohol 99.7%, acetone 98%, Polyvinylpyrrolidone (PVP, MW: 1000–130000) were supplied from Tianjin Kermel Chemical Reagent Co. Ltd. Pt/C catalysts (20 wt%, Johnson Matthey). To prepare the aqueous solutions, Wahaha Pure Water from Wahaha Group Co. Commercial. All reagents were used without further purification.

2. Methods

2.1 Synthesis of Pd NWs

In a typical synthesis, an aqueous solution containing water (15 mL), $PdCl_2$ (17.7 mg) , NaI (300 mg) and PVP (1000 mg) was added into a 50-mL small beaker, transferred the homogeneous dark red mixtures to a 20 mL Teflon-lined stainless-steel autoclave after the liquid aqueous solution is completely dissolved under ultrasonic, and heated at 205 ℃ for 155 minutes in the preheated oven, after self-cooling to room temperature, we gathered the the Pd nanowires by centrifugation under 9000 rpm, and washed it twice by ethanol/acetone mixture, and then dispersed it in ethylene glycol for further use at a concentration of 0.4 $mg \cdot mL^{-1}$.

2.2 Synthesis of $PdPt_3Ir_1$ porous NTs

In a typical process, PVP (350 mg), NaI (150 mg), AA (25 mg), the suspension of Pd nanowires (3 mL) and 20 mL ethylene glycol were mixed in a 100-mL round-bottom flask, and preheated in oil bath at 110 ℃ for 20 min. A solution containing ethylene glycol (8 mL), H_2PtCl_6 (5 mg), $IrCl_3$ (5 mg) and PVP (300 mg) was added to the round-bottom flask at a rate of 1 mL/h use burette, at the same time, the reaction temperature rose to 200℃ and then kept the solution at 200 ℃ for 1 h, after cooling to room temperature, we gathered the $PdPt_3Ir_1$ porous NTs by centrifugation under 9000 rpm, and washed it twice by ethanol/acetone mixture, then the obtained nanowires were dispersed in ethanol for further use. The route for the synthesis of $PdPt_mIr_n$ NTs were nearly the same with that for the $PdPt_3Ir_1$ NTs, except for the precursor solution was changed the concentration of H_2PtCl_6 and $IrCl_3$. The product yield is about 85-90% (mass fraction).

2.3 Preparation of PdPtIr porous NTs/C- 400

The PdPtIr porous NTs/C catalyst was prepared by mixing carbon and the as-synthesized PdPtIr porous NTs in ethanol under magnetically stirring overnight at room temperature. Then, the mixed solution is thermal annealing under N_2 atmosphere at 400℃ for 2h to obtain the PdPtIr porous NTs/C-400.

3. Instruments

The morphology and structure of various nanocrystals were performed with transmission electron microscopy (TEM) on HITACHI HT7700 at an accelerating voltage of 120 kV. A Thermo Scientific ESCALAB 250Xi photoelectron spectrometer with a Mg-Kα as the exciting source (1253.6 eV) was analyzed the X-ray photoelectron spectroscopic (XPS) spectral. X-ray diffraction (XRD) patterns were conducted using a Rigaku D/MAX-2500 powder diffractometer with Cu-KαX-ray source at the speed of 4°/min between 10 and 100 degrees (~2θ) by. High-angle annular dark-field scanning transmission electron microscopy (HAADF-STEM), high-resolution TEM (HRTEM) and atomic energy dispersive X-ray spectroscopy (EDS) were carried out on Thermo Fisher Scientific C-FEG (200 KV). Inductively coupled plasma atomic mass spectrometer (ICP-AES) (710-ES, Varian) was used to obtain the compositions of the catalysts. In-situ EDS-mapping of heating experiment was recorded at HITCHI HF5000.

4. Electrochemical measurements

All the electrochemical measurements were carried out by using CHI 760E electrochemical workstation (Shanghai Chenhua Instrument Corporation, China) in a three-electrode system by using a glassy carbon Rotating Disk Electrode (RDE, diameter: 5 mm, area: 0.196 cm^2) as the working electrode. An Ag/AgCl electrode and a platinum plate were used as reference and counter electrodes, respectively. Before the

electrochemical measurement, all the catalysts were dispersed into mixture of isopropanol/ water/ Nafion solution at 1:0.95:0.05 volume ratio obtaining a homogeneous catalyst ink with a concentration of 0.2 mg Pd+Pt+Ir/mL by sonicating, then the glassy carbon electrode (GCE) was polished with alumina slurry and cleaned with ethanol and water several times. 10 uL catalyst ink was carefully added dropwise on the surface of the GEC. The cyclic voltammetry (CV) curves were recorded in a N_2-saturated 0.1 M $HClO_4$ aqueous solution in the potential range of 0.05-1.1V vs. RHE at a scanning rate of 50 $mV \cdot s^{-1}$. Electrochemical active surface areas (ECSAs) were determined from the charge associated with the adsorption of hydrogen from 0.05-0.4 V after double-layer correction with a reference value of 210 $\mu C \cdot cm^{-2}$. The oxygen reduction reaction (ORR) and oxygen evolution reaction (OER) measurements were performed at room temperature using RDE at a scan rate of 10 mV s−1 with a rotating speed of 1600 rpm in an O_2-saturated 0.1 M $HClO_4$. The data were corrected by 90% ohmic iR drop compensation. The accelerated durability tests (ADTs) were recorded at in the range of 0.6 V - 1.1 V versus RHE in O_2-saturated 0.1 M $HClO_4$ solution. Before measurement, the catalysts were stabilized and cleaned by pre-scanning between 0.05 and 1.1 V versus RHE in a saturated N_2 atmosphere 0.1 M $HClO_4$ for 1000 cycles at a scan rate of 500 mV/s. The kinetic current was calculated based on the derived Koutecky-Levich equation:

$$1/i=1/i_k +1/i_d$$

Where i is the current experimentally measured at 0.9 V vs. RHE, ik and id are the kinetic current and diffusion-limiting current. Mass activity (MA) was obtained by normalizing the kinetic current to the amount of loaded Pd+Pt+Ir and specific activity (SA) was obtained by normalizing the ECSA value.

5. DFT calculations

Periodic density function theory (DFT) calculations have been performed using the Vienna Ab Initio Simulation Package (VASP). The exchange-correlation energy and potential are described by the generalized gradient approximation in the form of PBE. Plane waves with a cut-off of 400 eV are used for projector augmented wave (PAW) potentials. The criteria for the convergence are the residual force less than 0.02 eV Å-1. The thickness of the vacuum layer is 15 Å. Based on the EDS results, the atomic ratio of Pt:Pd is set to 1:1 for PtPd surface and Pt:Pd:Ir is 7:7:2 for PtPdIr surface. The optimized lattice constants of bulk PtPd and PtPdIr are 3.96 Å and 3.95 Å, respectively. The smaller lattice constant of bulk PtPdIr compared to bulk PtPd, is assigned to smaller atomic radius of Ir (1.27 Å) than those of Pt (1.30 Å) and Pd (1.28 Å). The effect of spin polarization is considered during the calculations. The K points mesh was set by Monkhorst-Packing method as 7 x 8 x 1 for PtPd(211)(1x2) and PtPdIr(211)(1x2) surfaces and 4x8x1 for PtPd(311)(2x2) and

PtPdIr(311)(2x2) surfaces with 7-layer slabs, respectively. The top four layers are relaxed, while the three bottommost layers are fixed at their bulk positions.

6. Figures

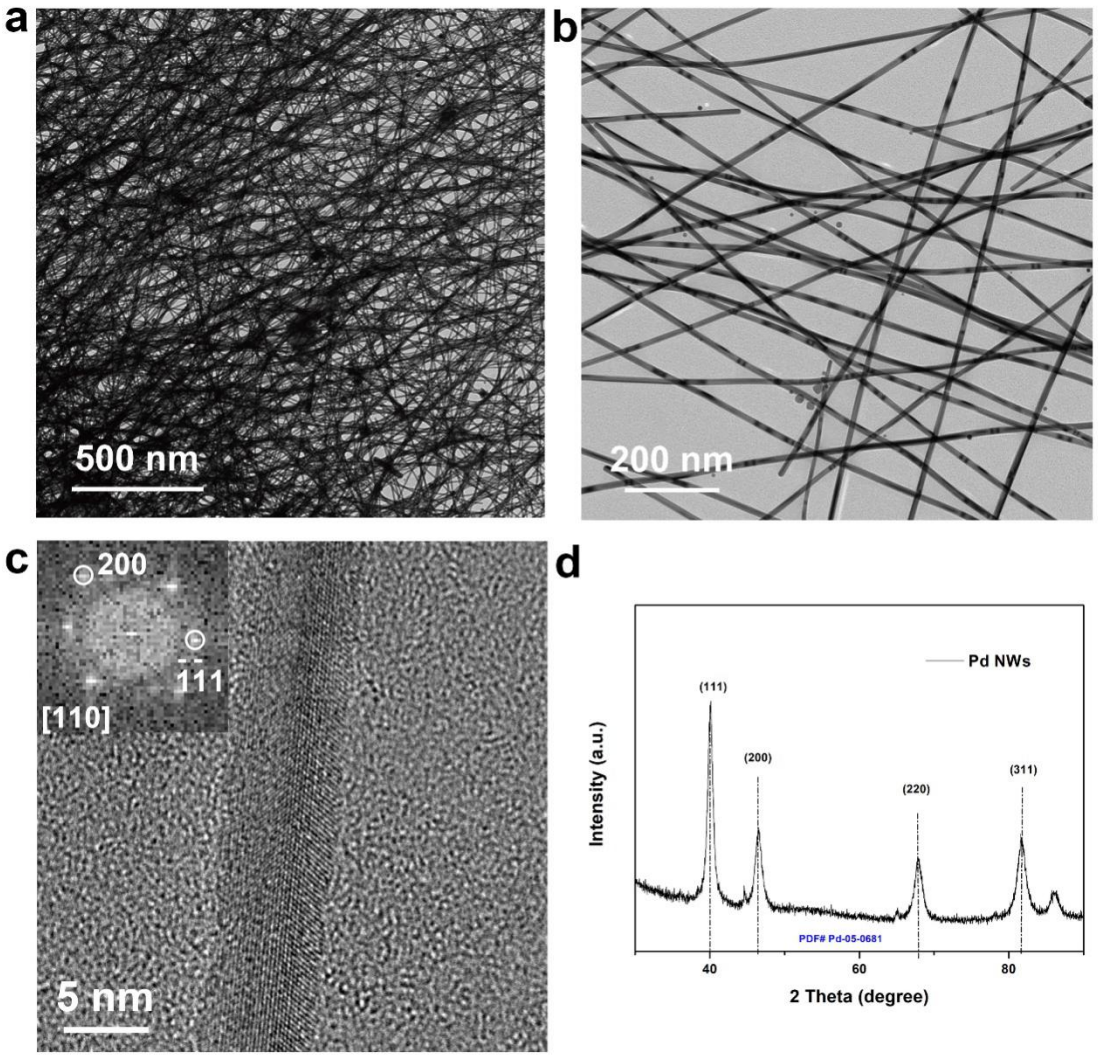

Figure S1. (a, b) TEM images, (c) HRTEM image, (d) XRD of pre-prepared smooth Pd nanowires.

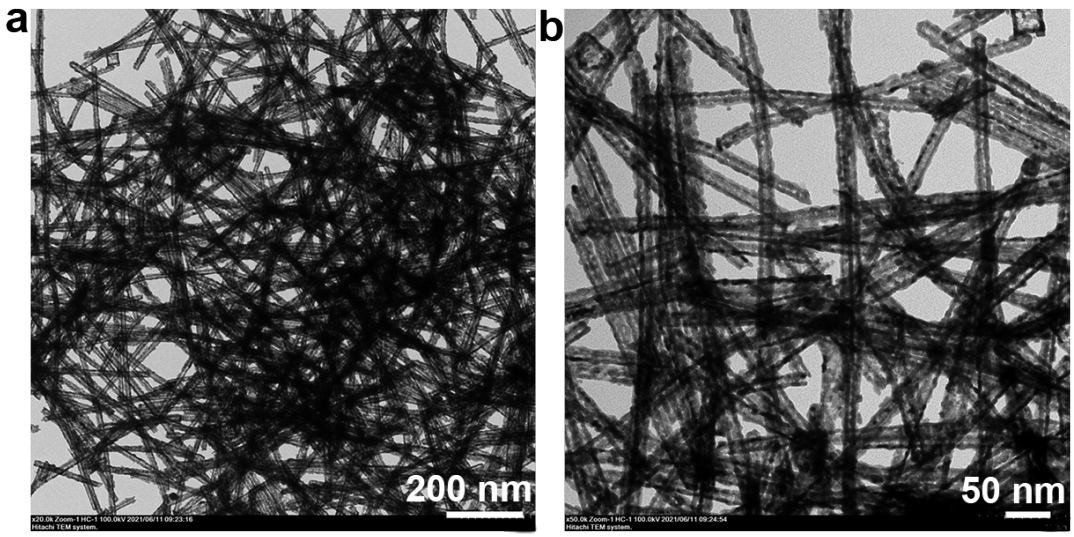

Figure S2. TEM images of plentiful PdPtIr PNTs in low(a) and high(b) magnifications.

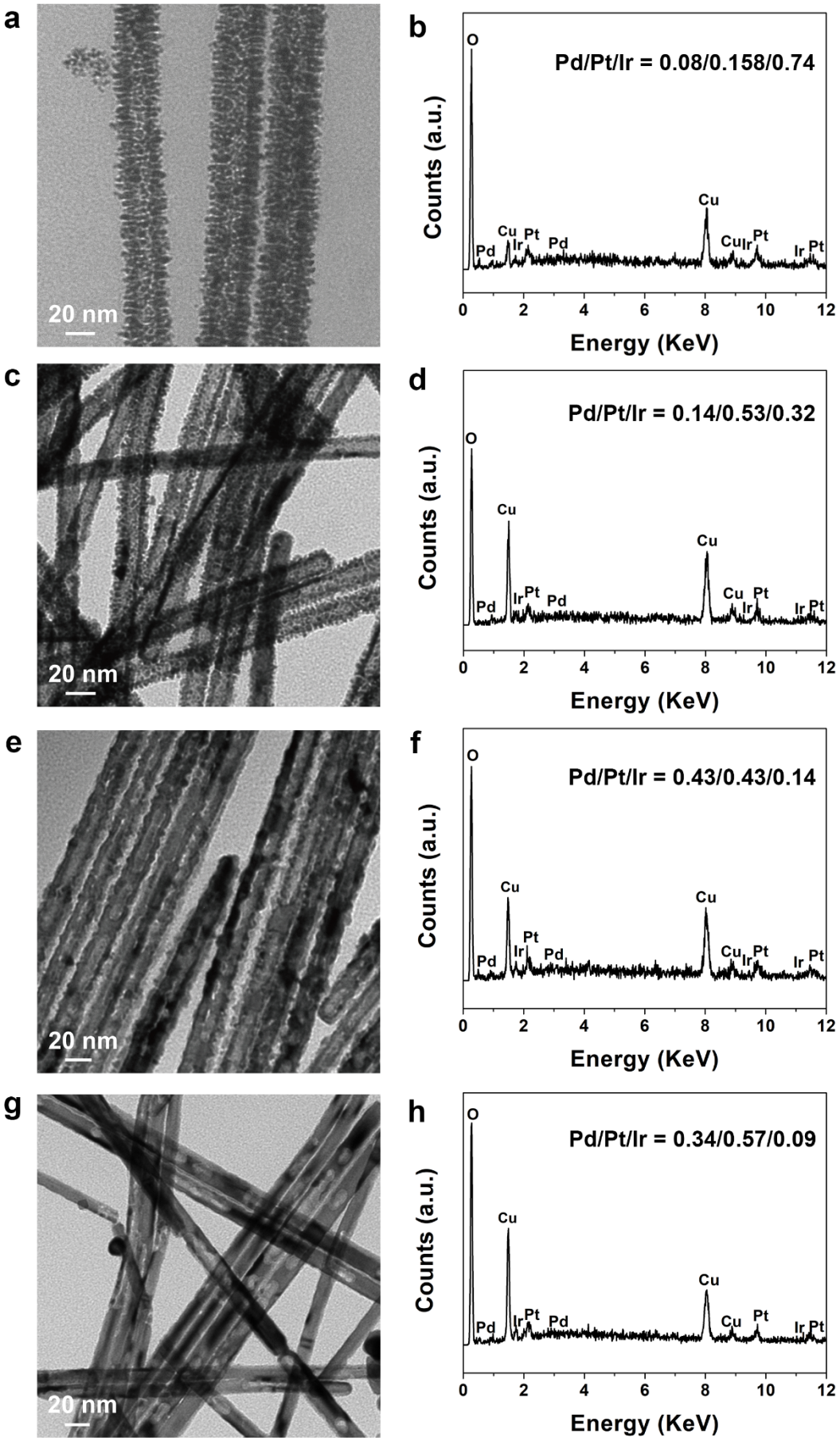
a
20 nm
b
Pd/Pt/Ir = 0.08/0.158/0.74
Counts (a.u.)
Energy (KeV)
c
20 nm
d
Pd/Pt/Ir = 0.14/0.53/0.32
Counts (a.u.)
Energy (KeV)
e
20 nm
f
Pd/Pt/Ir = 0.43/0.43/0.14
Counts (a.u.)
Energy (KeV)
g
20 nm
h
Pd/Pt/Ir = 0.34/0.57/0.09
Counts (a.u.)
Energy (KeV)

Figure S3. TEM images and corresponding TEM-EDS of products with the same conditions as those of PdPtIr PNTs except the feeding Pt/Ir precursor ratio. (a,b) 1:5 of Pt: Ir. (c,d) 2:1 of Pt: Ir. (e,f) 3:1 of Pt: Ir. (g,h) 5:1 of Pt: Ir.

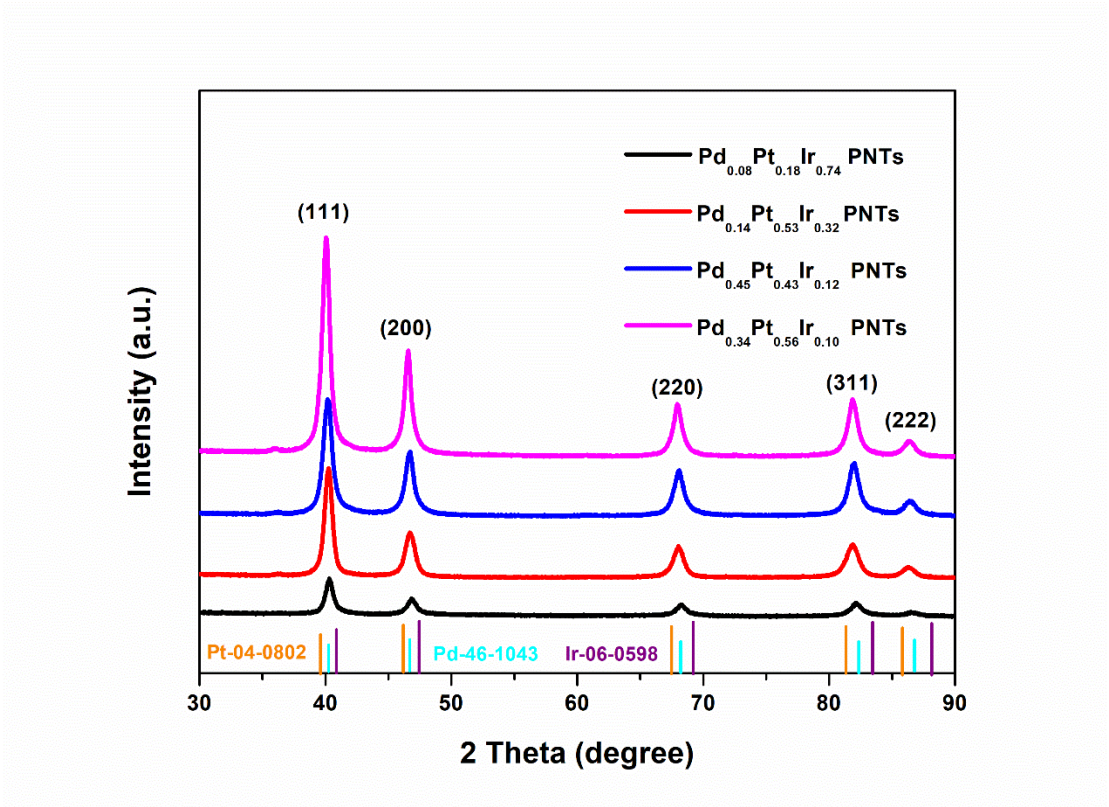

Figure S4. XRD pattern of PdPtIr PNTs with Pt/Ir precursor feed ratio of 1/5, 2/1, 3/1, 5/1.

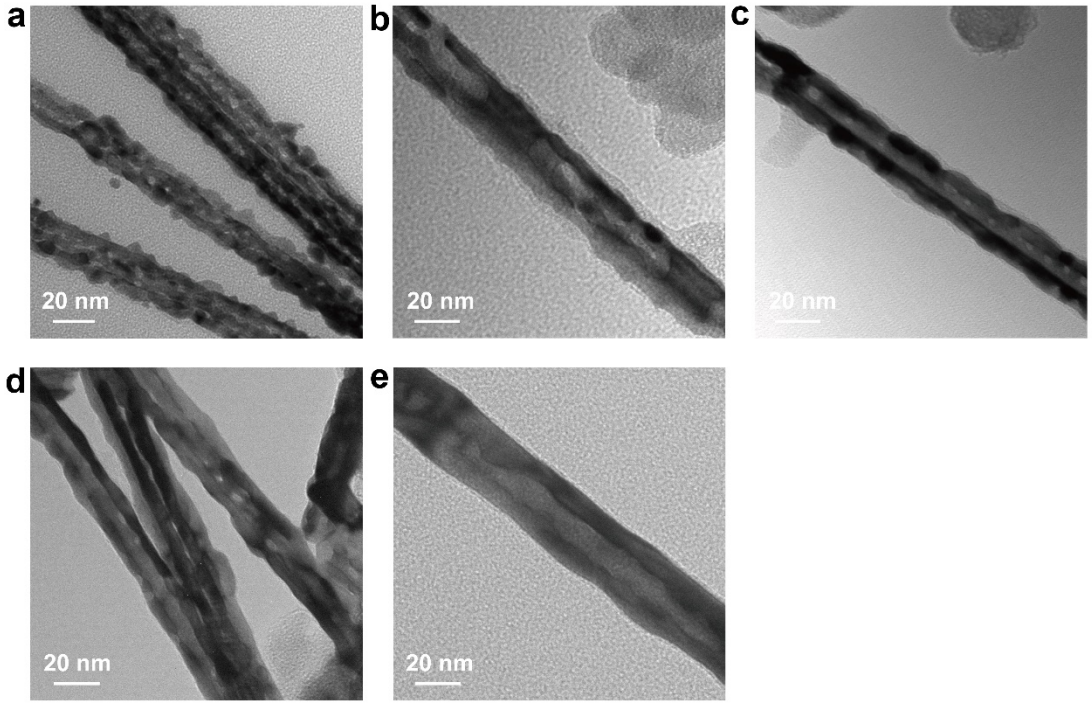

Figure S5. (a) TEM images of PdPtIr PNTs before, and (b) after annealing at 350 ℃, (c) 400 ℃, (d) 450 ℃ and (e) 500 ℃. With increasing annealing temperature, the rough surfaces of NWs gradually disappear, resulting in smooth surfaces.

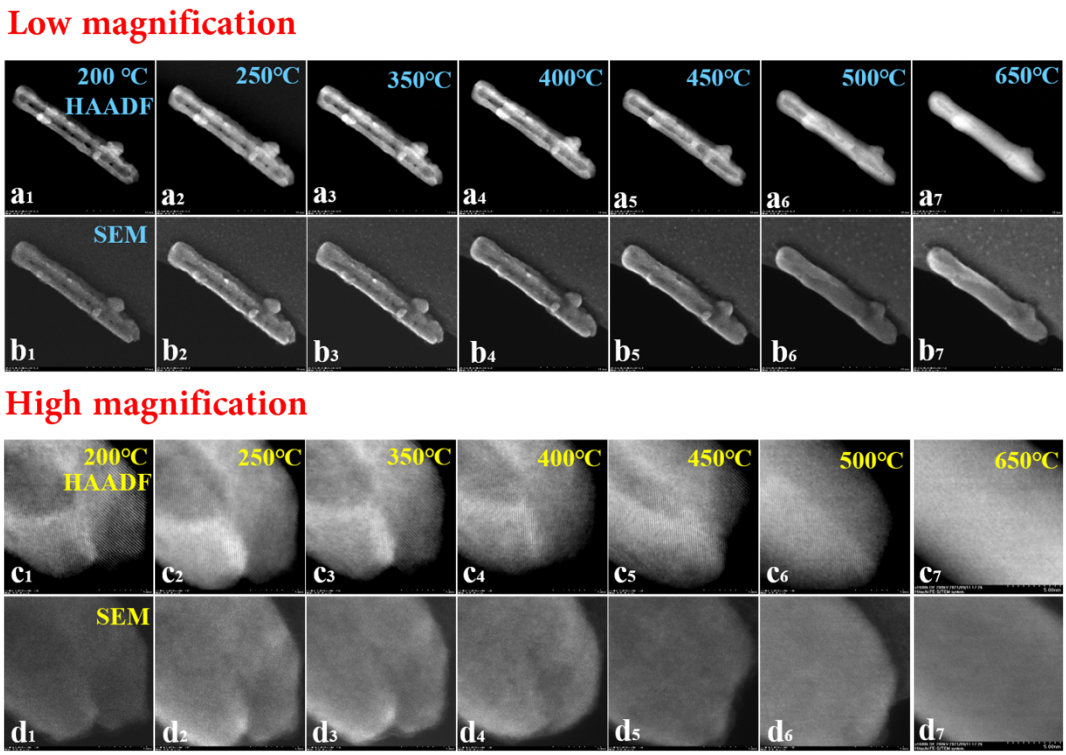

Figure S6. Seven different temperatures from 200 ℃ to 600 ℃ for detailed in-situ heating experiments. At low magnification (a1-b7), only the overall change in PNTs with the increase of temperature can be observed. However, at high magnification (c1-d7), we can see that the top of the PNTs begins to change at 250°C, while the sidewall of the PNTs begins to change around 400°C. At 450 °C, the morphological characteristics of the PNTs changed completely. At 500 °C, the pores in the PNTs disappeared.

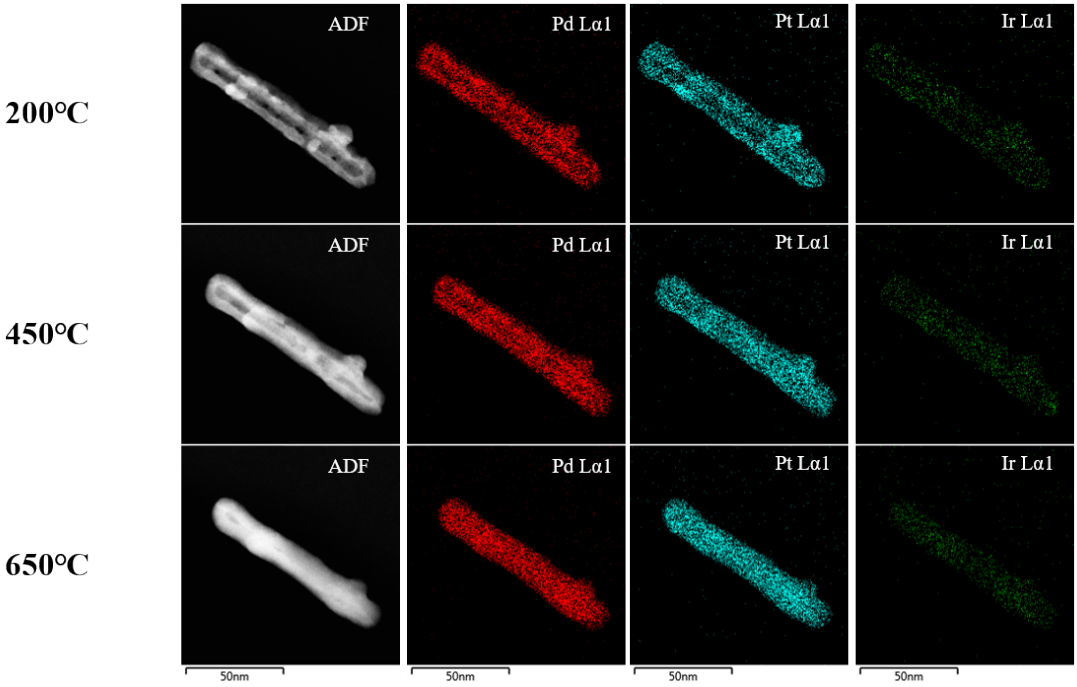

Figure S7. In-situ EDS-mapping images of heating experiment to explore the effect of calcination temperature on PdPtIr PNTs. It is found that as the temperature increases, the edges of the nanowires gradually become smooth.

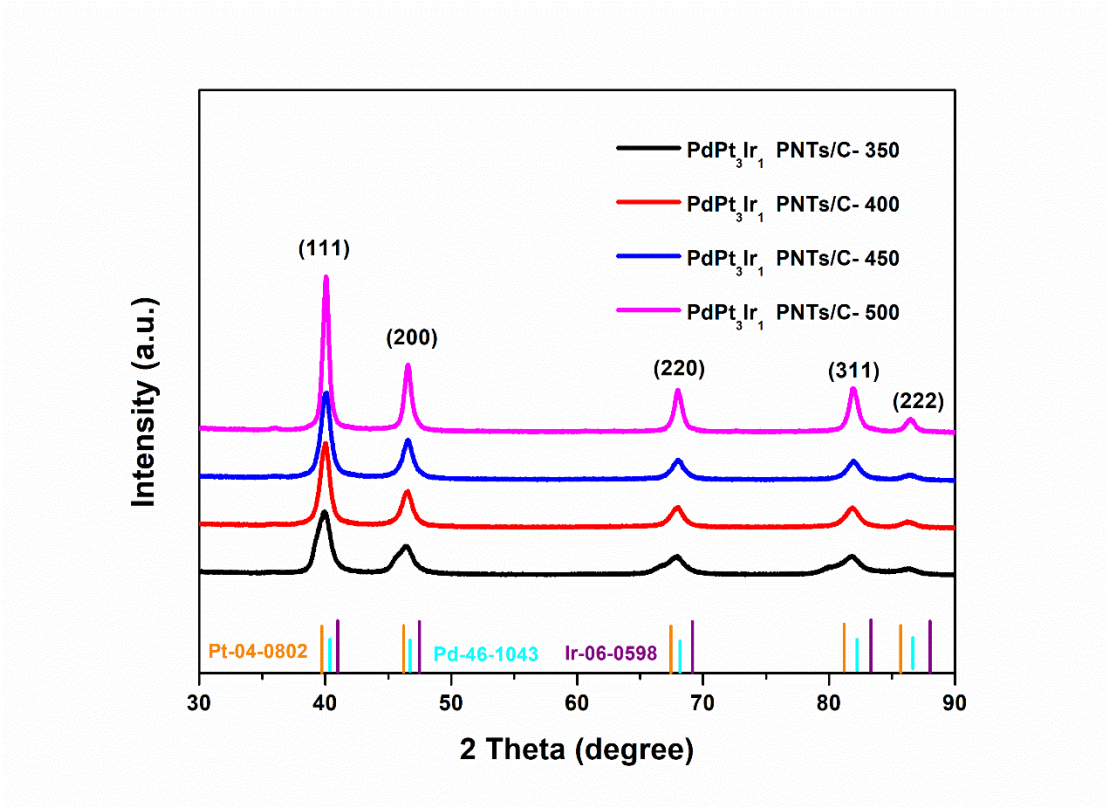

Figure S8. XRD pattern of PdPtIr PNTs-(350-500).

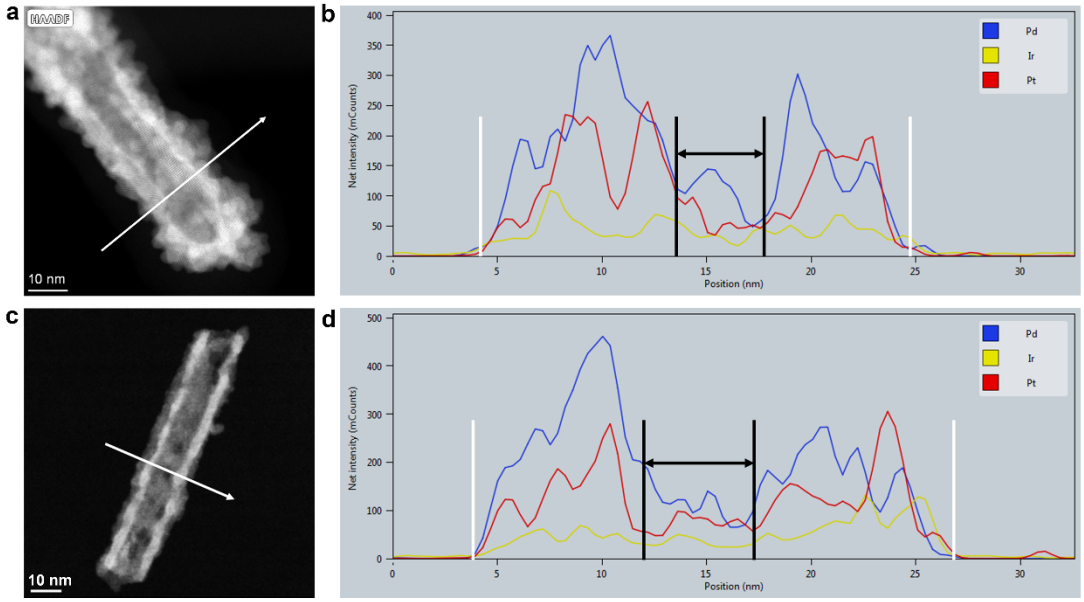

Figure S9. (a, b) Line scan analysis of PdPtIr-PNTs, (c, d) Line scan analysis of PdPtIr-PNTs/C-400. the radial line scan the PdPtIr-PNTs (Figure S9a, marked with white arrows), and Figure S9d shows the radial line scan of the PdPtIr-PNTs/C-400 (Figure S9c, marked with white arrows). The presence of Pd, Pt, Ir and inner diameter (about 5 nm) provided direct evidence of PdPtIr PNTs and PdPtIr-PNTs/C-400 nanoarchitectures.

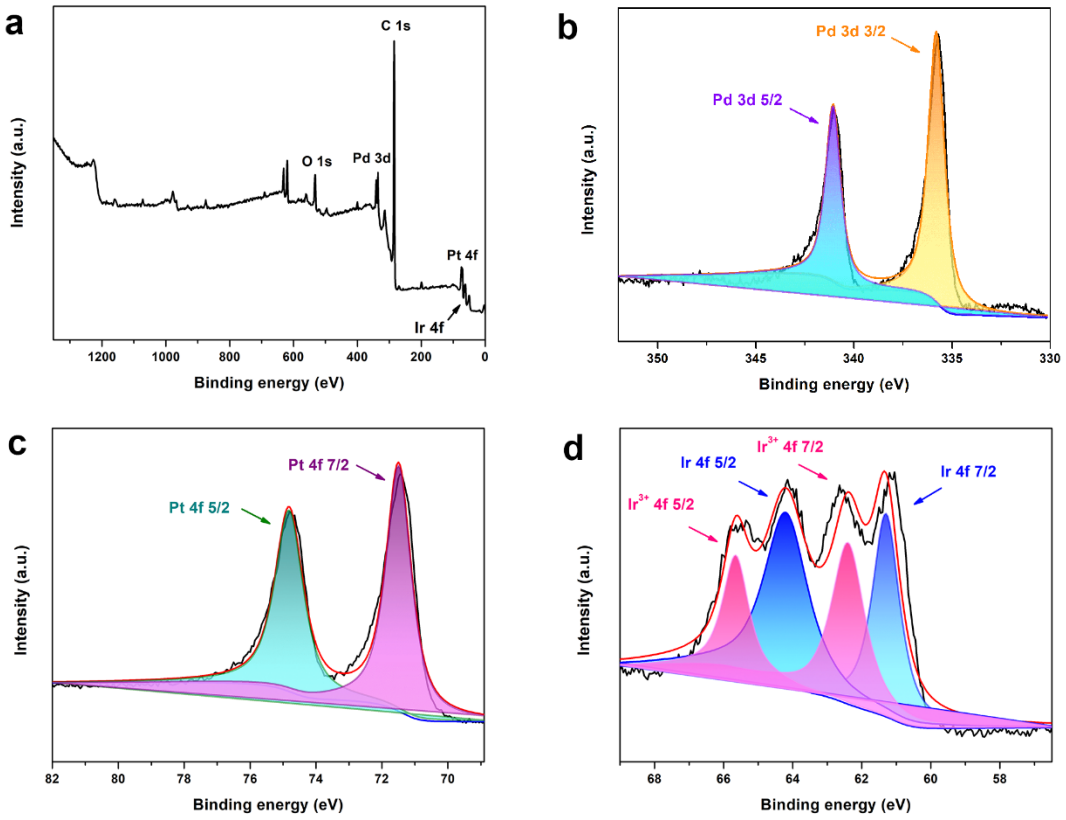

Figure S10. XPS spectra of PdPtIr PNTs- 400. (a) XPS survey, (b) Pd 3d, (c) Pt 4f, and (d) Ir 4f.

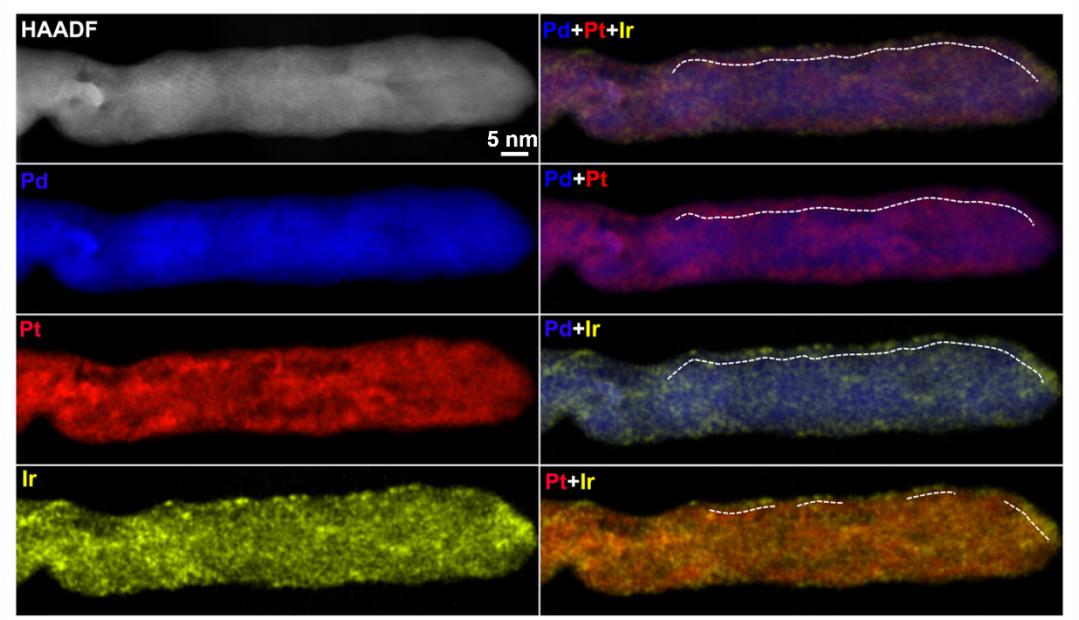

Figure S11. STEM-EDS elemental mapping of the PdPtIr PNTs/C-400.

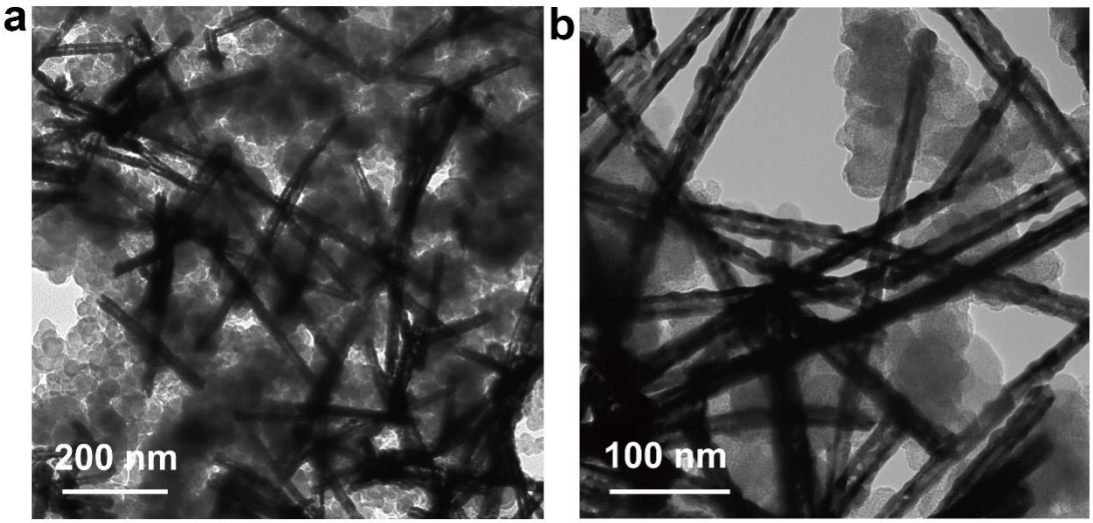

Figure S12. TEM images of (a) PdPtIr PNTs/C and (b) PdPtIr PNTs/C-400. Which are well-proportioned deposited on the XC-72 carbon support without structural or composition change.

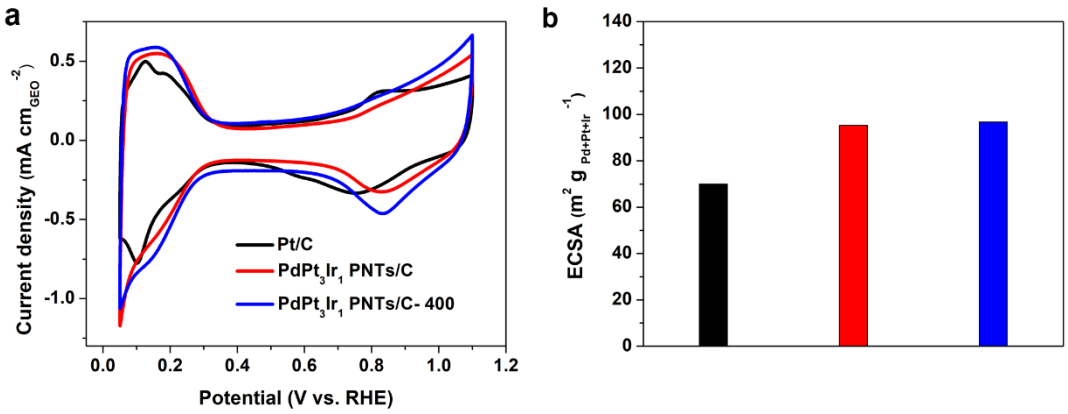

Figure S13. (a) Cyclic voltammograms and (b) Histogram of ECSA for different catalysts.

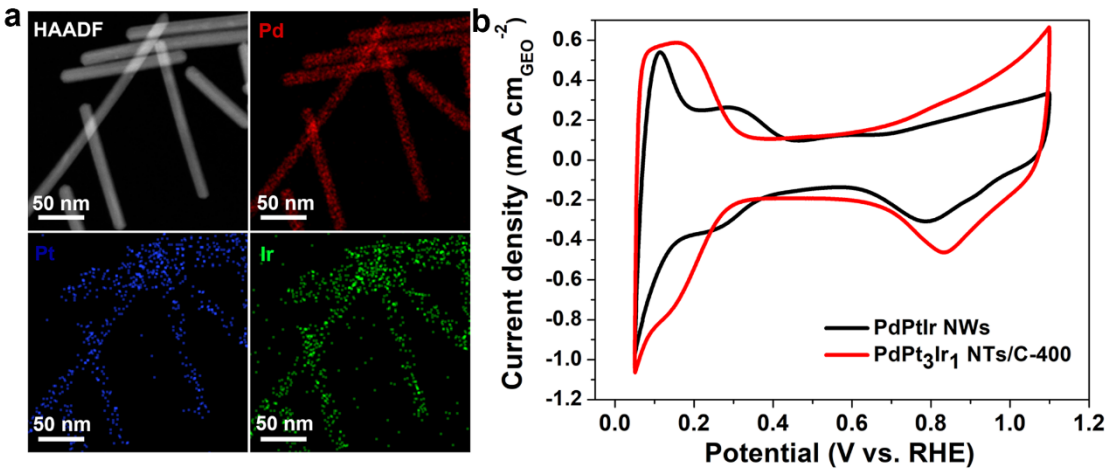

Figure S14. (a) STEM-EDS elemental mapping of the PdPtIr NWs. (b) CVs of PdPtIr NWs and PdPtIr PNTs/C- 400.

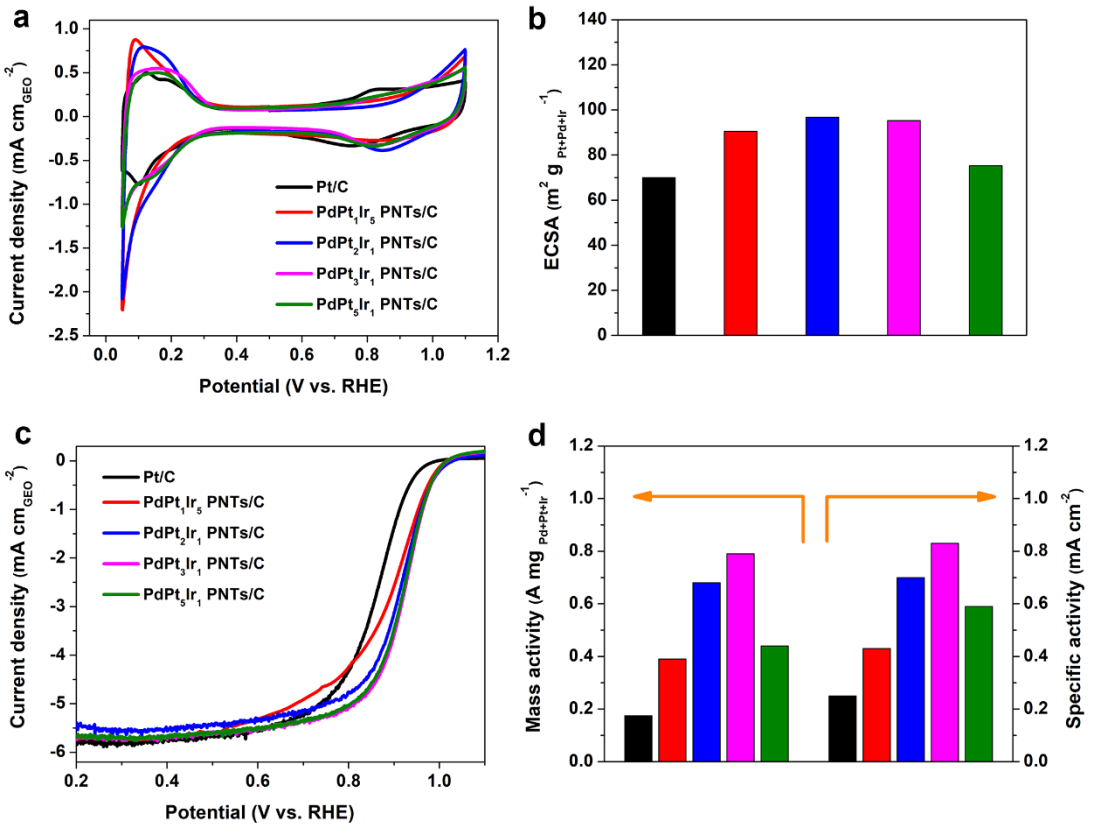

Figure S15. (a) Cyclic voltammograms and (b)Histogram of ECSA of PdPtIr PNTs/C catalysts synthesized with Pt/Ir feeding ratio of 1/5, 2/1, 3/1, 5/1. (c) ORR polarization curves and (d) Histogram of MA and SA of PdPtIr PNTs/C catalysts synthesized with Pt/Ir feeding ratio of 1/5, 2/1, 3/1, 5/1. Commercial Pt/C was used as the benchmark catalyst.

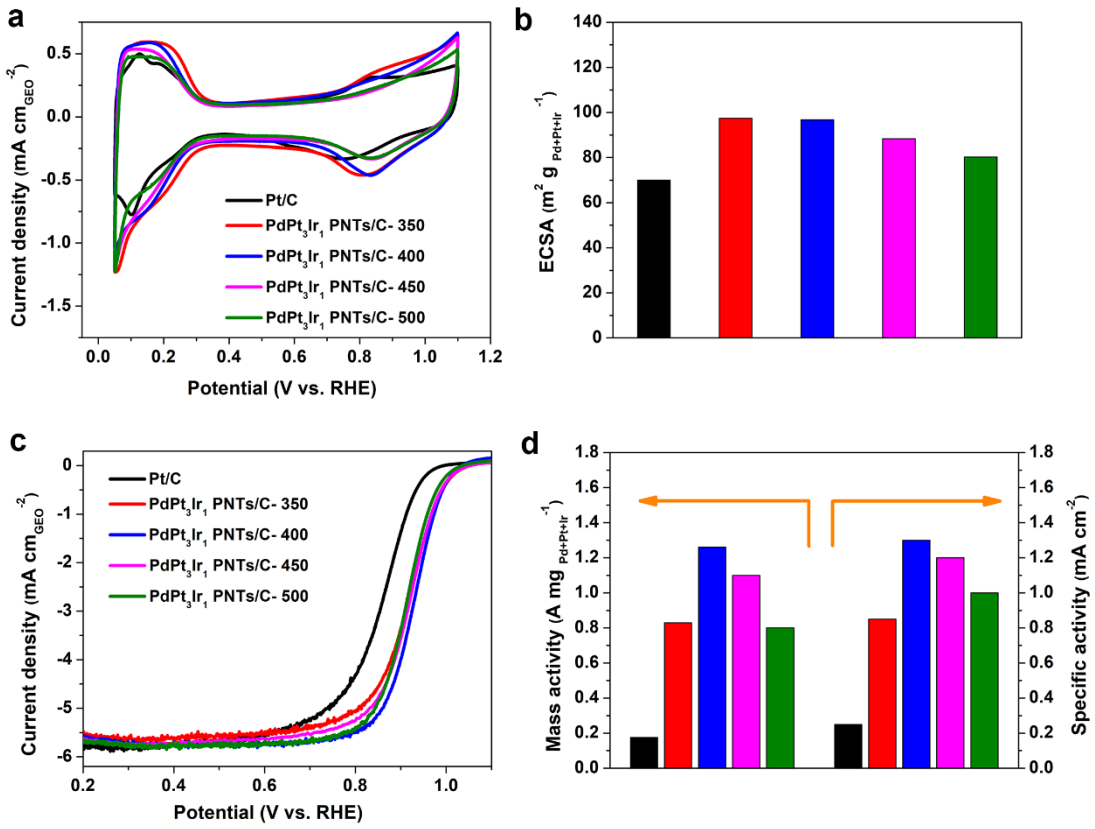

Figure S16. (a) Cyclic voltammograms and (b) Histogram of ECSA of PdPtIr PNTs/C catalyst annealed under 350 ℃, 400 ℃, 450 ℃, 500 ℃. Commercial Pt/C was used as the benchmark catalyst. (c) ORR polarization curves and (d) Histogram of MA and SA of PdPtIr PNTs/C catalysts annealed under 350 ℃, 400 ℃, 450 ℃, 500 ℃. Commercial Pt/C was used as the benchmark catalyst.

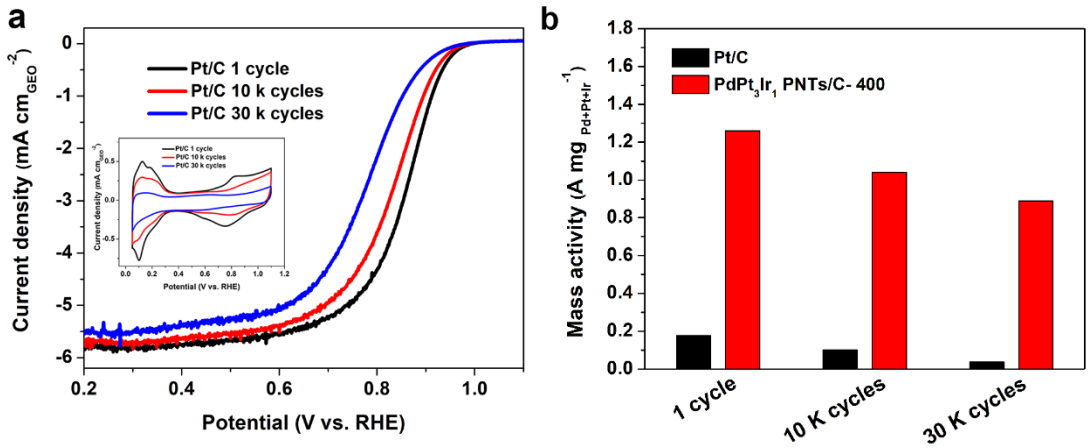

Figure S17. (a) Cyclic voltammograms and ORR polarization curves of commercial Pt/C catalyst before and after 10 000 and 30 000 potential cycles between 0.6 and 1.1 V versus RHE. (b) MA of PdPtIr PNTs/C-400 and commercial Pt/C before and after 10 000, 30 000 potential cycles between 0.6 and1.1 V versus RHE.

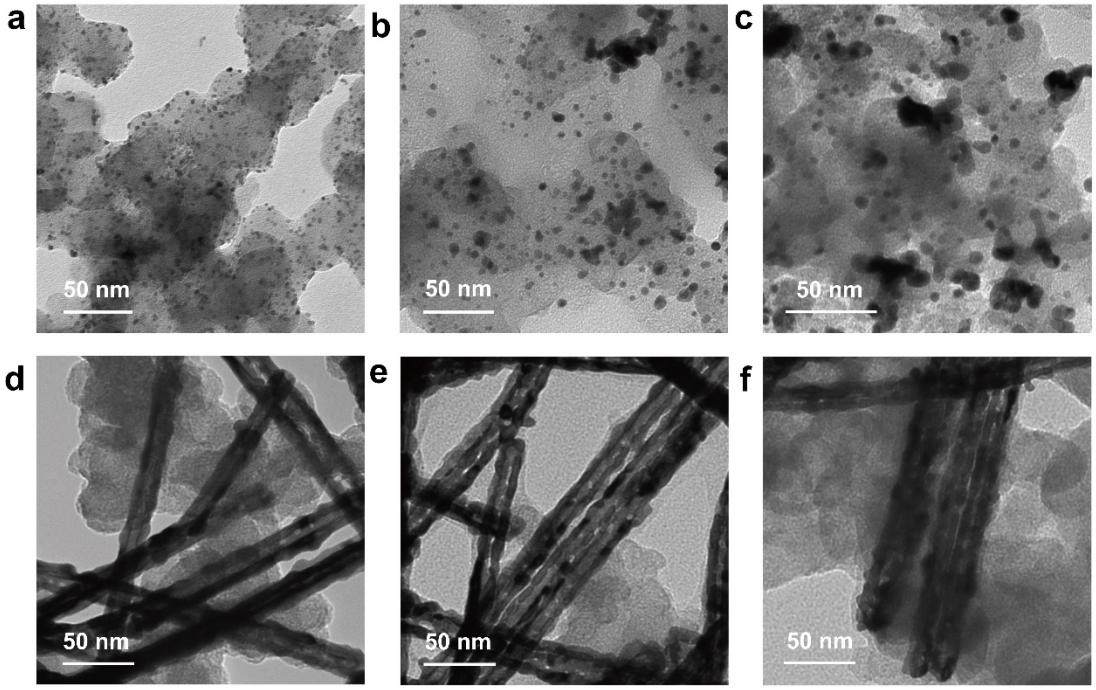

Figure S18. (a-c) TEM images of commercial Pt/C catalyst before and after 10000 and 30000 potential cycles between 0.6 and 1.1 V versus RHE. (d-f) TEM images PdPtIr PNTs/C- 400 catalyst before and after 10 000 and 30 000 potential cycles between 0.6 and 1.1 V versus RHE.

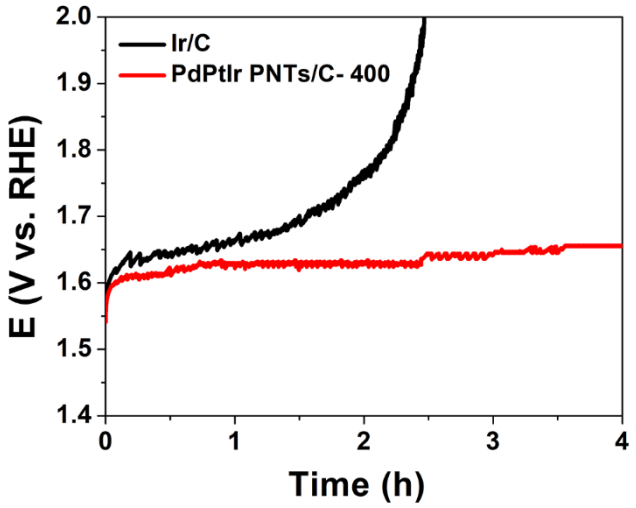

Figure S19. OER chronopotentiometry curves at 10 mA/cm^2 of PdPtIr PNTs/C- 400 and Ir/C in 0.1 M H_2ClO_4.

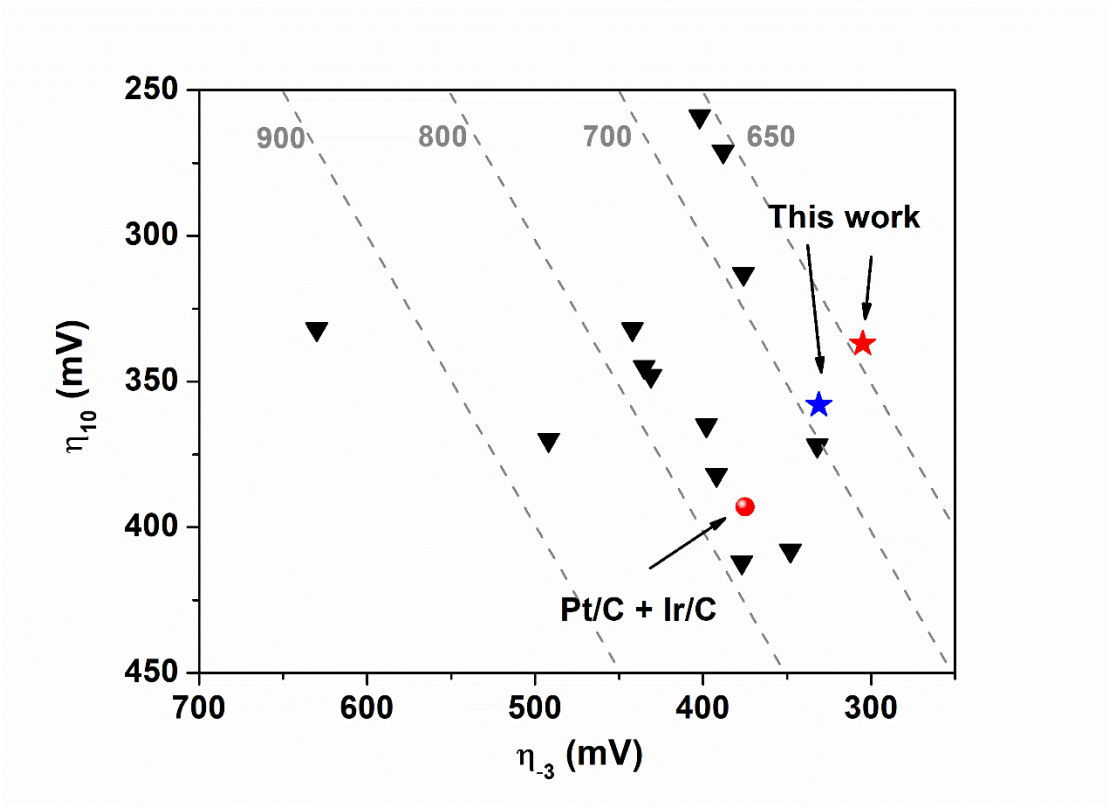

Figure S20. The dual catalysts activity of PdPtIr PNTs/C-400 on ORR and OER, and the dual catalysts activity of other dual-catalysts used in acid media reported in the literature.

7. Tables

Catalyst	PdPtIr (atomic ratio)	Pd (atomic ratio)	Pt (atomic ratio)	Ir (atomic ratio)
$PdPt_1Ir_5$ PNTs/C	1	0.120	0.168	0.712
$PdPt_2Ir_1$ PNTs/C	1	0.145	0.543	0.312
$PdPt_3Ir_1$ PNTs/C	1	0.428	0.433	0.139
$PdPt_5Ir_1$ PNTs/C	1	0.380	0.528	0.092

Table S1. The content of various metals in the catalyst by ICP.

Catalyst	ECSA ($m^2\ g_{Pd+Pt+Ir}^{-1}$)	Mass activity ($A\ mg_{Pd+Pt+Ir}^{-1}$)	Specific activity ($mA\ cm^{-1}$)
Pt/C	70	0.175	0.25
$PdPt_5Ir_1$ PNTs/C	90.6	0.39	0.43
$PdPt_2Ir_1$ PNTs/C	96.7	0.68	0.7
$PdPt_3Ir_1$ PNTs/C	95.3	0.79	0.83
$PdPt_1Ir_5$ PNTs/C	75.2	0.44	0.59

Table S2. ECSA**,** MA, and SA of various catalysts.

Catalyst	ECSA ($m^2 g_{Pd+Pt+Ir}^{-1}$)	Mass activity ($A mg_{Pd+Pt+Ir}^{-1}$)	Specific activity ($mA cm^{-1}$)
Pt/C	70	0.175	0.25
$PdPt_3Ir_1$ PNTs/C- 350	97.5	0.83	0.85
$PdPt_3Ir_1$ PNTs/C- 400	96.7	1.26	1.3
$PdPt_3Ir_1$ PNTs/C- 450	88.4	1.1	1.24
$PdPt_3Ir_1$ PNTs/C- 500	80.3	0.8	1

Table S3. ECSA**,** MA, and SA of various catalysts.

Catalyst	ADT	ECSA ($m^2 g_{Pd+Pt+Ir}^{-1}$)	Mass activity ($A mg_{Pd+Pt+Ir}^{-1}$)
Pt/C	1 cycle	70	0.175
$PdPt_3Ir_1$ PNTs/C- 400		96.7	1.26
Pt/C	10 K cycles	45.7	0.1
$PdPt_3Ir_1$ PNTs/C- 400		87.5	1.19
Pt/C	30 K cycles	13.3	0.037
$PdPt_3Ir_1$ PNTs/C- 400		85	0.89

Table S4. ECSA and MA of Pt/C and $PdPt_3Ir_1$ PNTs/C- 400 before and after 10 000, 30 000 potential cycles between 0.6 and1.1 V versus RHE.

Catalyst	Loading ($\mu g\ cm^{-2}_{geo}$)	Electrolyte	η-3 (mV)	η10 (mV)	ΔE (mV)	Ref
$Pt_{3.1L}/Ir_{1.3L}$ nanocages	10.2	0.1 M $HClO_4$	376	313	689	1
$Pt_{1.4L}/Ir_{3.1L}$ nanocages	10.2	0.1 M $HClO_4$	388	271	659	1
$Pt_{3.2L}/Ir_{1.4L}$ nanocages	10.2	0.1 M $HClO_4$	402	259	661	1
Pt-Pd-Ir nanocages	16.8	0.1 M $HClO_4$	332	372	704	2
Pt-Pd-Ir nanocages	8.4	0.1 M $HClO_4$	348	408	756	2
$Ir_{67}@Pt_{33}$ nanodendrites	38	0.5 M H_2SO_4	492	370	862	3
Pt/Ir_9O_{18} nanoparticles	380	0.5 M H_2SO_4	442	332	774	4
Pt/IrO_2 nanoparticles	380	0.5 M H_2SO_4	431	348	779	4
Pt_3/Ir_7O_{14} nanoparticles	380	0.5 M H_2SO_4	435	345	780	4
Pt-Ir/TiC	122	0.1 M $HClO_4$	377	412	789	4

$PtIr/Ti_4O_7$	N/A	0.5 M H_2SO_4	392	382	774	5
Pt-Ir nanocrystals	50	0.5 M H_2SO_4	630	332	962	6
rGO-supported Pt-Ir	145	0.1 M $HClO_4$	398	365	763	7
Pt/C+Ir/C	10	0.1 M $HClO_4$	375	393	768	This work
PdPtIr PNTs	10	0.1 M $HClO_4$	331	358	689	This work
PdPtIr PNTs-400	10	0.1 M $HClO_4$	305	337	642	This work

Table S5. The ORR-OER performance of the dual catalysts in acidic electrolyte.

8. References

1. Zhu, J.; Xu, L.; Lyu, Z.; Xie, M.; Chen,R.; Jin, W.; Mavrikakis, M.; Xia, Y. Janus Nanocages of Platinum-Group Metals and Their Use as Effective Dual-Electrocatalysts. *Angew. Chem., Int. Ed.* **2021**, *60*, 10384–10392.
2. Zhu, J.; Xie, M.; Chen, Z.; Lyu, Z.; Chi, M.; Jin, W.; Xia, Y. Pt-Ir-Pd Trimetallic Nanocages as a Dual Catalyst for Efficient Oxygen Reduction and Evolution Reactions in Acidic Media. *Adv. Energy Mater.* **2020**, *10* (16), 1904114.
3. da Silva, G. C.; Fernandes, M. R.; Ticianelli, E. A. Activity and Stability of Pt/IrO 2 Bifunctional Materials as Catalysts for the Oxygen Evolution/Reduction Reaction. *ACS Catal*. **2018**, *8* (3), 2081–2092.
4. Fuentes, R. E.; Colón-Mercado, H. R.; Martínez-Rodríguez, M. J. Pt-Ir/TiC Electrocatalysts for PEM Fuel Cell/Electrolyzer Process. Journal of The Electrochemical Society. **2013**, *161* (1), F77–F82.
5. Won, J.-E.; Kwak, D.-H.; Han, S.-B.; Park, H.-S.; Park, J.-Y.; Ma, K.-B.; Kim, D.-H.; Park, K.-W. PtIr/Ti_4O_7 as a bifunctional electrocatalyst for improved oxygen reduction and oxygen evolution reactions. *Journal of Catalysis*. **2018**, *358*, 287–294.
6. Zhang, T.; Li, S. S.; Zhu, W.; Zhang, Z.; Gu, J.; Zhang, Y. Shape-tunable Pt-Ir Alloy Nanocatalysts with High Performance in Oxygen Electrode Reactions. *Nanoscale* **2017**, *9*, 1154.

7. Kim, I. G.; Nah, I. W.; Oh, I.-H.; Park, S. Crumpled rGO-supported Pt-Ir bifunctional catalyst prepared by spray pyrolysis for unitized regenerative fuel cells. *Journal of Power Sources*. **2017**, *364*, 215–225.